Chapter 4

Verification – Intercomparison of Terrestrial Radiative Transfer

The evaluation of terrestrial radiative transfer modeling with SARTre is based on a series of cases increasing in complexity. The intercomparison will start with a "simple" clear-sky radiative transfer case taking into account only molecular absorption and emission (case I), presented in section 4.3. Furthermore, in section 4.4 a cloud case will be examined, where only thermal emission is considered as source of radiation, whereas multiple scattering is neglected (case II).

The main part of the verification will deal with the intercomparison of radiative transfer modeling in a cloudy atmosphere taking into account both the thermal emission and the multiple scattering source term (case III). The scattering case aims at evaluating the validity of the pseudo-spherical assumption in SARTre, which has been explained in chapter 3. That involves the investigation of a monochromatic radiance field in and around the cloud for a plane-parallel and a spherical atmosphere additionally to the limb spectra analyzed for the other two cases. The results of case III along with a more detailed description of the different examined aspects are presented and discussed in section 4.6. Preliminary to the scattering model intercomparison, some SARTre internal consistency tests of the implementation of the scattering source in SARTre itself and of the integration of the radiative transfer solver DISORT are presented (section 4.5).

Prior to the intercomparison results, section 4.1 introduces the models MIRART, KOPRA, and ARTS, which SARTre has been intercompared to. Section 4.2 describes the setup of the atmospheric properties and parameters as well as the observation geometries that are examined.

4.1 Models in the Intercomparison

Three radiative transfer modeling packages, MIRART, KOPRA, and ARTS are used for the verification of SARTre. Although all the packages incorporate more than radiative transfer modeling abilities, only the forward modeling parts are involved in this intercomparison. Each of these models is used for a subset of cases in the intercomparison, according to their individual features. An overview of the capabilities of the models is given in the following subsections. Characteristics relevant to the intercomparison are described in detail.

4.1.1 MIRART

MIRART, the **M**odular **I**nfra**R**ed **A**tmospheric **R**adiance and **T**ransmission package, is "a suite of programs for high resolution infrared atmospheric radiative transfer with emphasis on efficient and reliable numerical algorithms and a modular approach for simulation and/or retrieval in a variety of applications" (Schreier and Schimpf, 2001). MIRART has been verified by intercomparisons in the AMIL2DA (**A**dvanced **MI**PAS **L**evel **2** **D**ata **A**nalysis) project (von Clarmann et al., 2002) and in the IRTM workshops (Melsheimer et al., 2005).

The forward modeling by MIRART includes the line-by-line calculation of molecular absorption cross sections (for more details see section 3.2 about SARTre's LbL module, that has been adapted from MIRART) and the solution of the integral forms of the Beer and Schwarzschild equations (Eqs. (2.3) and (2.8)) by means of numerical quadrature schemes. From the quadrature schemes implemented in MIRART, the trapezoid scheme (MIRART-Trapez) and a quadrature using the piecewiese cubic Hermite interpolant of the integrand (MIRART-Hermite), have been applied. Since absorption/emission and scattering by particulate matter (aerosol and hygrosols) is not taken into account by MIRART, it is only used for case I, the comparison of clear-sky limb spectra.

4.1.2 KOPRA

KOPRA (Stiller et al., 2002), the **K**arlsruhe **O**ptimized and **P**recise **R**adiative transfer **A**lgorithm, is "a numerically optimized line-by-line-algorithm simulating all significant physical processes of radiative transfer in the gaseous atmosphere for various observation geometries" (Höpfner, 2004). KOPRA is furthermore capable of considering processes due to aerosols and clouds. That includes absorption and emission as well as scattering of radiation in and out of the line of sight. Scattering into the line of sight (LOS) is restricted to single scattering processes.

KOPRA solves the integral form of the radiative transfer equation (RTE), given by Eq. (2.7), using a layer-by-layer approach. For each path segment of the LOS passing a single layer, absorber column amounts and mass weighted pressure and temperature are determined. From these, path segment representative molecular absorption cross sections for individual molecules are calculated. Furthermore, average aerosol optical properties are derived. Absorption and extinction cross sections as well as phase functions in dependency of size parameter and refractive index of the aerosols are provided by an aerosol model based on Mie theory, that has been included in KOPRA.

Finally, Eq. (2.7) is solved considering source terms J_B (Eq. (2.10)) and J_MS (Eq. (2.11)). Assuming homogeneous conditions along the path segment, the source function integral can be solved analytically, resulting in

$$I = \frac{1}{\bar{\beta}_\mathrm{e}}(\bar{\beta}_\mathrm{a}\,\bar{B} + \bar{\beta}_\mathrm{s}\,\bar{I}_\mathrm{s})(1 - e^{-\bar{\beta}_\mathrm{e}\,\Delta s}), \tag{4.1}$$

with $\bar{\beta}_\mathrm{a} = \bar{\beta}_\mathrm{a}^\mathrm{mol} + \bar{\beta}_\mathrm{a}^\mathrm{par}$ and $\bar{\beta}_\mathrm{s} = \bar{\beta}_\mathrm{s}^\mathrm{par}$ denoting the path segment averaged absorption and scattering coefficient, respectively. Δs is the path length of the segment, $\bar{B}$ the Planck function of average path segment temperature, and $\bar{I}_\mathrm{s}$ represents the solution of the scattering integral Eq. (3.31). The derivation of $\bar{I}_\mathrm{s}$ is based on an incident radiation field, which has been calculated for a variety of angles for each path segment by solving Eq. (4.1) but neglecting scattering therein. That means, for the incident radiation field only thermally emitted radiation is considered as

source, but attenuation includes absorption and scattering out of the path. In conclusion, beside thermal emission, first order or single scattering of radiation can be modeled.

The clear-sky RT part of KOPRA has been verified extensively by intercomparisons, e.g. by Glatthor et al. (1999) and in the AMIL2DA project (von Clarmann et al., 2002) , where MIRART took part as well. Furthermore, single scattering KOPRA has been used for data analysis of measurements of polar stratospheric clouds (Höpfner et al., 2002).

Although KOPRA is able to model single scattering, for the comparison with SARTre KOPRA has only been used for cases I and II. This is because no separation of SARTre modeled intensities into first and higher order scattering is possible.

However, cloud optical properties used for cases II and III of this intercomparison have been derived from the aerosol model implemented in KOPRA. Additionally, molecular absorption cross sections calculated by KOPRA have been used by ARTS for the RT simulations, that are presented here.

4.1.3 ARTS

ARTS (Buehler et al., 2005), the **A**tmospheric **R**adiative **T**ransfer **S**imulator, is an extensive package of modules for radiative transfer modeling and applications in the millimeter and sub-millimeter spectral range, whose latest version includes, e.g., the **D**iscrete **O**rdinate **IT**erative (DOIT) scattering method for solving the vector RTE (Emde, 2005). Basically, the scattering version of ARTS is a full spherical three-dimensional RT model considering polarization effects. But, within this intercomparison only 1D, scalar radiative transfer modeling is used with molecular absorption cross sections taken from KOPRA.

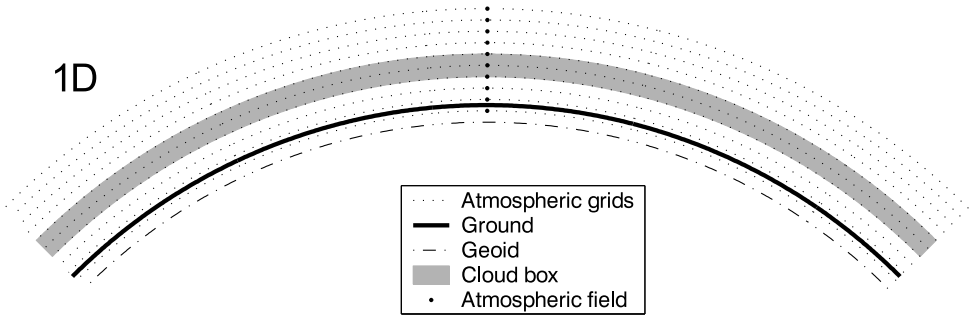

Figure 4.1: *The cloud box and atmospheric grids in ARTS for a 1D atmospheric setup. Note that the cloud box has to enclose the cloud(s), but the cloud box is not the cloud. Usually, the cloud box is chosen larger than the cloud, for example to avoid scattered radiation to reenter the cloud box.*

In order to reduce computational efforts, scattering calculations in ARTS are restricted to a finite part of the atmosphere containing clouds and other scattering objects, the so-called cloud box (see Fig. 4.1). Outside the cloud box, the radiative transfer is calculated on the basis of the Schwarzschild equation (Eq. (2.8)). Depending on the viewing geometry and atmospheric condition, the background term $I(0)$ is given by the cosmic background (clear-sky limb or uplooking observations), the upwelling radiation from the ground (clear-sky downlooking observations), outgoing radiation from the cloud box (cloud observation from outside the cloud) or the internal intensity field of the cloud box (observer inside the cloud). The Schwarzschild equation is

applied separately to individual path segments and solved analytically under the assumption of homogeneous conditions within a single path segment:

$$I_n = I_{n-1}\, e^{-\bar{\beta}_\mathrm{e}\,\Delta s} + (1 - e^{-\bar{\beta}_\mathrm{e}\,\Delta s})\bar{\beta}_\mathrm{e}^{-1}(\bar{\beta}_\mathrm{a}\,\bar{B}), \tag{4.2}$$

where $\bar{\beta}_\mathrm{e}$, $\bar{\beta}_\mathrm{a}$ and $\bar{B}$ are path segment averaged quantities of extinction and absorption coefficients and the Planck function, respectively, and I_n denotes the intensity at path grid point n. Basically, ARTS solves the vector RTE, i.e. $\bar{\beta}_\mathrm{e}$ and $\bar{\beta}_\mathrm{a}$ are single elements of the extinction matrix $\boldsymbol{K}$ and the absorption vector $\boldsymbol{a}$. However, for scalar clear-sky radiative transfer applies $\bar{\beta}_\mathrm{e} = \bar{\beta}_\mathrm{a}$.

The task of the scattering part of ARTS is to determine the outgoing intensity field of the cloud box, which is used as background radiation term I_0 when the line of sight intersects the cloud box. The scattering calculations are restricted to the cloud box. Hence, all scattering objects, including reflecting surfaces, have to be inside the cloud box volume. The incident clear-sky intensity field provides the boundary conditions to the scattering RT problem. That means, the size of the cloud box has to be chosen in a way, that no radiation emerging from the cloud box might reenter.

For solving vector RT within the cloud box, two numerical methods have been implemented: a Monte Carlo scheme (Davis et al., 2005) and the iterative DOIT method (Emde, 2005), that has been used for the intercomparison. ARTS-DOIT starts with the calculation of the scattering integral Eq. (3.31) for all points within the cloud box, using a first guess incident radiation field $\boldsymbol{I}^{(0)}$, deriving the scattered radiation field $\boldsymbol{S}^{(0)}$. Following that, the RT equation is solved for discrete directions within single layers. Due to spherical geometry, the new radiation field has to be interpolated to the original angular grid, resulting in radiation field $\boldsymbol{I}^{(1)}$. Finally, convergence is checked between $\boldsymbol{I}^{(0)}$ and $\boldsymbol{I}^{(1)}$. If the convergence criterion is not met yet, $\boldsymbol{I}^{(1)}$ is used for the incident radiation field guess and the process is repeated until it converges.

Generally, for solving the scattering integral a rather coarse equidistant angular grid is used. In contrast to that, the intensity fields are calculated for a finer grid with dense grid points around horizontal direction, where the radiation field is strongly increasing with slightly increasing zenith angle. The fine angular grid is defined by an optimization procedure, finding an optimal grid to represent the clear-sky field within the cloud box, which is assumed to be the intensity field, that varies fastest around horizontal direction.

The LbL module of ARTS as well as the clear-sky RT has been intercompared to other models, e.g. MIRART, in the IRTM workshops (Melsheimer et al., 2005). ARTS-DOIT has furthermore been used to study the multiple scattering effects in mid-IR (Höpfner and Emde, 2005) and polarization effects induced by spherical particles in the microwave region (Teichmann et al., 2006).

Within this intercomparison, ARTS has been used for comparison of cases I and III. It has not been considered for case II, since scattering and emission terms are not separated when calculating the outgoing field of the cloud box.

4.2 Intercomparison Setup

The intercomparison setup is taken from Höpfner and Emde (2005). This setup was designed to analyze the influence of scattering on infrared radiation spectra from limb observations. Emphasis was placed on studying the validity of the single scattering approach used in KOPRA in comparison to the multiple scattering model ARTS-DOIT. Albeit, the setup meets the demands

of verifying the SARTre model along with investigating its limits due to the pseudo-spherical assumption in an ideal way.

In general, monochromatic spectra have been examined, i.e. no instrumental effects like field-of-view and instrumental line shape have been considered. Limb observations with tangent altitudes of 4, 6, 8, 10 and 11 km are modeled. In addition to limb spectra, intensity fields have been evaluated in sections 4.5 and 4.6. Modeling results are interpreted on the basis of percentage differences of intensity values, with SARTre used as the reference model:

$$\Delta I_{\%} = \frac{(I_{\text{other}} - I_{\text{SARTre}})}{I_{\text{SARTre}}} \cdot 100\%. \tag{4.3}$$

Thus, negative deviations denote an overestimation by SARTre compared to the "other" model – or an underestimation by the "other model" –, while positive differences mean a (relative) underestimation by SARTre.

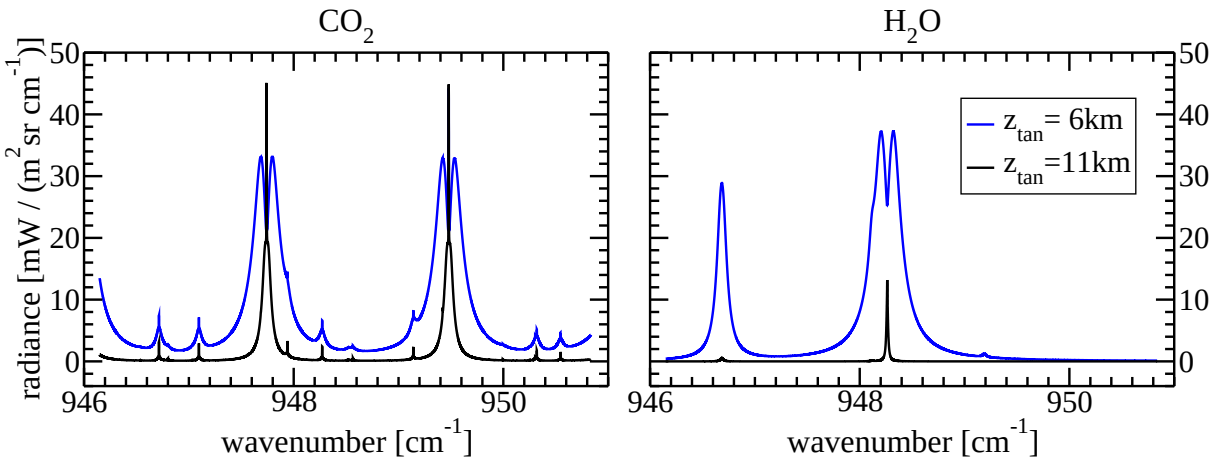

Figure 4.2: CO_2 *and* H_2O *lines in the spectral interval used for the intercomparison. Left panel shows spectra at 6 and 11 km tangent altitude when considering* CO_2 *only. Corresponding spectra for* H_2O *are presented in the right panel. Note the different behavior of* CO_2 *and* H_2O *lines concerning intensity and width of the lines in the higher and lower altitude spectra, respectively.* H_2O *content increases significantly in the atmosphere below 10 km, while* CO_2 *mixing ratio is constant (see Fig. 4.3).*

4.2.1 The Spectral Window

In accordance to Höpfner and Emde (2005), the spectral interval of $946.149 - 950.837\,\text{cm}^{-1}$ has been chosen for the intercomparison. This spectral region is located in the thermal infrared atmospheric window. Hence, a significant contribution from scattering by ice particles is expected. Intensity fields have been calculated at selected spectral positions. With their spectral placement, they are supposed to cover the variation of molecular absorption over the spectral interval examined throughout this chapter: one of them is located in the continuum region ($950.2\,\text{cm}^{-1}$), the others in the center and the wing of a CO_2 line ($947.8\,\text{cm}^{-1}$ and $947.6\,\text{cm}^{-1}$) and a strong H_2O line ($948.2\,\text{cm}^{-1}$ and $948.3\,\text{cm}^{-1}$), respectively.

4.2.2 Atmospheric Setup

The selected interval is characterized by two strong and some weaker lines of CO_2 and two H_2O lines (see Fig. 4.2). Absorption due to other molecules is low in the selected interval and is therefore neglected in the modeling. Furthermore, no molecular absorption continua are considered.

Due to the vertical distribution of water vapor in the atmosphere – 90 % of the total water vapor content is confined to altitudes below 6 km – H_2O lines are of special interest when studying or detecting high clouds in infrared spectra. While in case of clear-sky conditions water vapor lines are weak emission lines in limb observation spectra with tangent heights in the stratosphere and upper troposphere, they may change to absorption line type when scattering occurs and get broader than expected under upper troposphere conditions. As explained in section 2.4.4, these distinct spectral features result from scattering of radiation into the line of sight, which originates from the surface or lower troposphere. Consequently, the scattered fraction of radiation possesses spectral features characteristic of tropospheric radiation, like emission and absorption in wide, pressure broadened H_2O lines.

Standard profiles of CO_2 and H_2O as well as of temperature and pressure (see Fig. 4.3), defined on a 0.5 km grid up to 100 km, are used. The surface is assumed to be a blackbody ($\varepsilon = 1$) of the same temperature as assigned to the lowest altitude level.

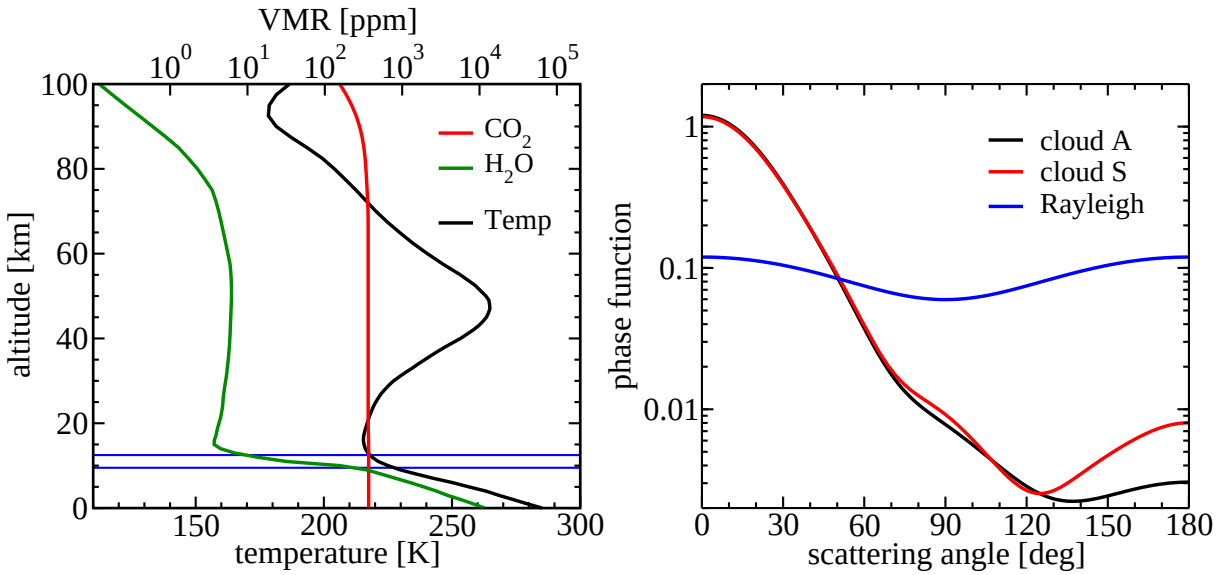

Figure 4.3: *Atmospheric profiles with blue lines indicating the position of the cloud layer (left). Phase function of "cloud A" and "cloud S" are shown compared to the Rayleigh phase function (right).*

4.2.3 The Clouds

Polar stratospheric clouds (PSCs), that occur in the stratosphere of the polar regions, are introduced as scattering medium. In contrast to cirrus clouds, PSCs usually contain small particles only. A log-normal size distribution with modal radius of 4 μm and a width of 0.3 is assumed. Single scattering properties are determined with the help of Mie calculations, based on refractive indices of ice presented by Toon et al. (1994). The resulting phase function is shown in Fig. 4.3.

The single scattering albedo is derived as $\omega_0 = 0.24$. That means, PSCs are strong absorbers in the chosen spectral interval, resulting from the interval located in the wing of an ice absorption band centered around 830 cm^{-1}. This cloud will be referred to as "cloud A" (absorbing cloud) in the following.

Beside the previously described strong absorbing cloud, referred to as "cloud A", a further, strong scattering "cloud S" has been created. Changing the complex refractive index m has lead to a single scattering albedo of $\omega_0 = 0.84$ and a slightly changed phase function (see Fig. 4.3). These two cloud types are appraised to cover a large fraction of the overall variability of ω_0 for various particle sizes over the infrared spectral range.[1]

The cloud is placed between 9.5 and 12.5 km altitude. By Höpfner and Emde (2005) the particle number density N of the cloud body between 10 and 12 km has been defined to be constant. From 9.5 to 10 km the number density increases linearly from 0 cm^{-3} to N, while from 12 to 12.5 km values decrease linearly.

Table 4.1: *Characteristics of cloud scenarios*

scenario	category	N	cloud A: ω_0=0.24		cloud S: ω_0=0.84	
		[cm^{-1}]	τ_z	$\tau_s(z_{tan}$=11 km)	τ_z	$\tau_s(z_{tan}$=11 km)
sc1	subvisible	0.01	$1.68{\cdot}10^{-3}$	0.170	$1.75{\cdot}10^{-3}$	0.176
sc2		0.1	$1.68{\cdot}10^{-2}$	1.70	$1.75{\cdot}10^{-2}$	1.760
sc3	moderate	1.0	$1.68{\cdot}10^{-1}$	17.0	$1.75{\cdot}10^{-1}$	17.60
sc4		10.0	$1.68{\cdot}10^{0}$	170.0	$1.75{\cdot}10^{0}$	176.0
sc5	opaque	100.0	$1.68{\cdot}10^{1}$	1700.0	$1.75{\cdot}10^{1}$	1760.0

Five scenarios with N varying from 0.01 cm^{-3} (scenario 1) to 100.0 cm^{-3} (scenario 5) in steps of one order of magnitude represent a reasonable range of cloud optical depths of approximately 0.0017 – 17 in nadir direction and 0.17 – 1700 in direction of limb path with tangent height of 11 km (see Tab. 4.1). That means, the cloud is totally opaque in nadir for scenario 5 only, but in limb for scenarios 3 to 5.

Since SARTre assumes particle number density to vary with altitude by an exponential function defined by the (virtual) number density at sea level N_0 and a scaling height H (see section 3.3), adequate density functions had to be fitted to the linearly varying functions given by Höpfner and Emde (2005). This has been done under the constraint of identical total particle number contained in the layer. Furthermore, the functions have been forced to have equal values at two points, placed 20 % of the layer geometrical thickness away from the layer boundaries ($N_{lin}(z_{low/high} \pm 0.2\Delta z) = N_{exp}(z_{low/high} \pm 0.2\Delta z)$).

For SARTre calculations, a "basic" layer setup was defined with just one layer in between 9.5 – 10.0 km and 12.0 – 12.5 km. For a second – "enhanced" – setup the 0.5 km layers have been divided into 5 sublayers with exponential number density functions fitted analogously for each sublayer. The creation of a second set of functions intended to fit the distribution of particles in the layer more closely to the original setup. To separately examine effects of increased number of layers and, consequentially, LOS grid points from effects of better fitting density functions, a third – "mixed" – setup has been created. This "mixed" setup has been defined with five

[1] Höpfner and Emde (2005) give a more elaborate evidence on that.

Table 4.2: *Setup of cloud layers to fit SARTre density functions to intercomparison setup definition. N_{lay} denotes the number of sublayers and N_{fct} is the number of density functions fitted to represent the whole layers.*

	9.5 – 10.0 km & 12.0 – 12.5 km		10.0 – 12.0 km	
setup	N_{lay}	N_{fct}	N_{lay}	N_{fct}
basic	1	1	4	1
mixed	5	1	4	1
enhanced	5	5	4	1

sublayers of identical N_0 and H for each of the sublayers, with N_0 and H taken from the "basic" setup (see Tab. 4.2). Resulting density number functions and integrated total particle numbers are illustrated in Fig. 4.4.

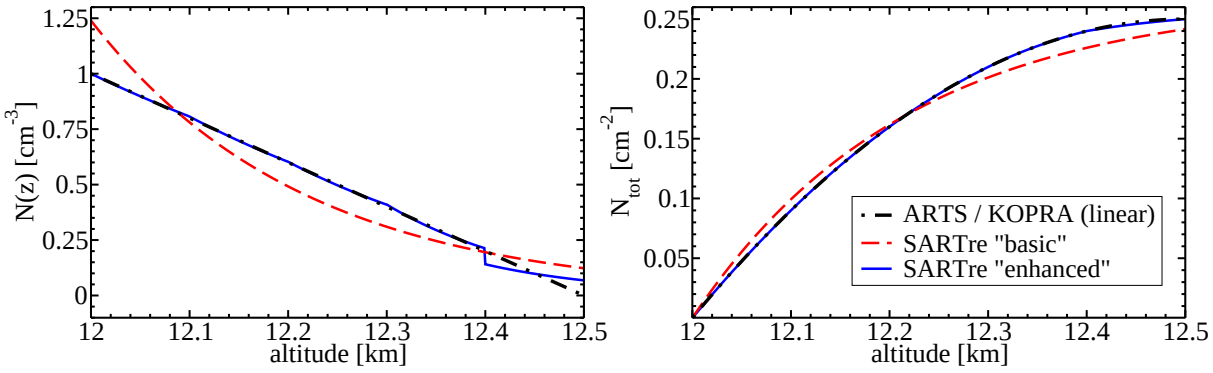

Figure 4.4: *Particle number density functions of the different cloud layer setups (left) and corresponding integrated total particle number (right) for the uppermost cloud layer.*

4.3 Case I – Clear-Sky Intercomparison

4.3.1 Motivation

The term "clear-sky" in radiative transfer refers to a particle free atmosphere, i.e. the atmosphere is considered to be composed of gaseous matter only. In infrared and microwave atmospheric radiative transfer the clear-sky assumption is usually seen as the standard case. For those clear-sky cases, it holds $\beta_{\mathrm{e}} \equiv \beta_{\mathrm{a}}^{\mathrm{mol}}$ and $\omega_0 = 0$. Thus, source term J simplifies to $J = J_{\mathrm{B}} = B(T)$ and the RTE (2.7) reduces to the Schwarzschild equation (2.8). From the Schwarzschild equation it is obvious, that thermal emission clear-sky radiances are a function of the atmospheric conditions along the line of sight only. Hence, clear-sky radiative transfer may be seen as the basic case of terrestrial radiative transfer – in the sense of representing the basic principle.

For the verification of SARTre, the intercomparison of clear-sky limb radiances is used to

- check the correctness of the implementation of LbL-modules of MIRART into SARTRe,
- verify the implementation of the source integration along the LOS
- ensure the SARTre model to be in sufficient agreement with KOPRA and ARTS for the comparisons of the more complex cases II and III.

Since the LbL modules of SARTre were adapted from MIRART (see section 3.2), the first two issues are addressed by comparing SARTre to MIRART with results discussed in subsection 4.3.2. Results concerning the latter item are presented in subsection 4.3.3.

All calculations have been done on the basis of the atmospheric setup described in 4.2, without considering a cloud. Limb radiance spectra for the five tangent altitudes between 4 and 11 km have been simulated and compared.

4.3.2 Results of the SARTre – MIRART Comparison

To check the integration of MIRART LbL-modules into SARTre, MIRART radiances were derived on the basis of molecular absorption coefficients calculated by MIRART itself on the one hand. On the other, absorption coefficients calculated by SARTre have been used as input to the source integration module of MIRART. Both methods result in identical limb radiance spectra for all tangent altitudes.

Results of the intercomparison of the RT modeling are shown in Fig. 4.5 for representative three out of the five limb paths. Since MIRART and SARTre base upon identical LbL-derived absorption coefficients, intensity deviations can be explicitly assigned to different approaches to the path integration. For the source integration by MIRART, two different numerical methods have been used – the trapezoidal rule and the Hermite quadrature scheme. Differences of about 1 – 2 % in average and up to 3 % between these two MIRART methods are observed. SARTre results can be found in between the two MIRART versions. With deviations of less than 0.5 % in average they are in good agreement with the MIRART-Hermite integration radiances. Largest differences occur in the flank of the water vapor line around 948.2 cm^{-1}.

4.3.3 Results of Comparing SARTre to KOPRA and ARTS

When comparing SARTre clear-sky spectra to KOPRA and ARTS (Fig. 4.5, lower panel), not only the methods of path integration differ, but also algorithms used to derive molecular absorption cross sections. Line-by-line algorithms may differ with regard to numerical solutions as well as to physical approaches like the particular line shapes or partition functions that have been implemented and the individual lines that have been considered in the spectral interval. When discussing the results, it has to be noted that KOPRA and ARTS use the same absorption cross sections, calculated by KOPRA. Hence, the deviations between KOPRA and ARTS spectra are due to their different approaches on source integration along the LOS.

Deviations between SARTre and KOPRA are found to be around 0.5 % in average at 11 km and around 1 % at lower tangent altitudes. SARTre and ARTS show differences of 1 % in average at 11 km and around 2 % at lower tangent altitudes. Maximum deviations occur in the flanks of the H_2O lines. They are found to reach values of up to 6 % for ARTS and 4 % for KOPRA at the tangent altitude of 10 km, i.e. at the atmospheric level from where water vapor content increases steeply with decreasing altitude.

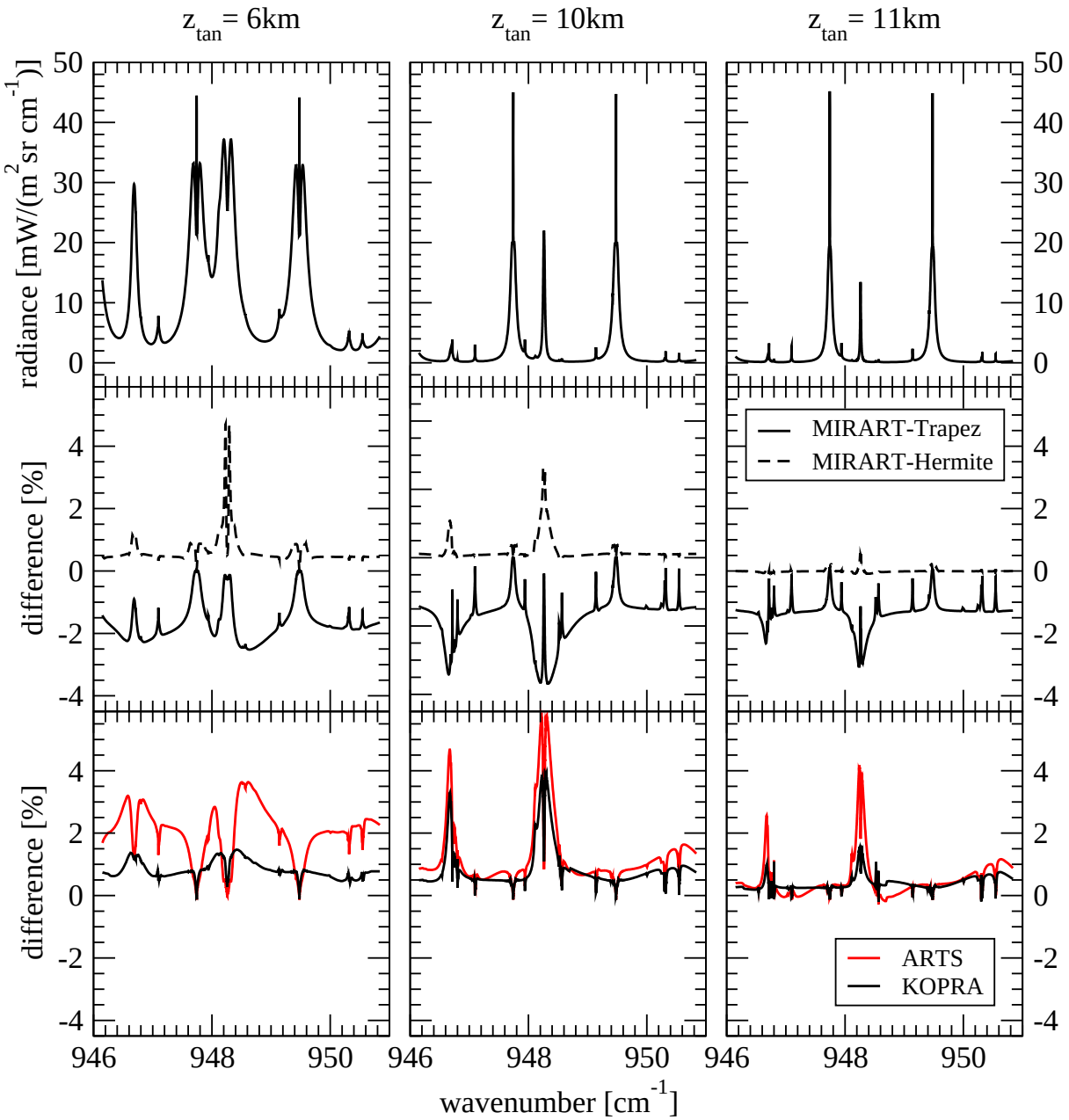

Figure 4.5: *Results of the intercomparison of IR clear-sky RT calculations are shown for tangent altitudes of 6 km (left), 10 km (center) and 11 km (right). SARTre spectra are shown in the upper panel, others are omitted since deviations are not noticeable in the radiance spectra. Center panel shows percentage deviations between SARTre and MIRART calculations using trapezoid and Hermite quadrature scheme. The lower panel illustrates differences between SARTre on the one hand, KOPRA and ARTS on the other.*

Although magnitudes of deviations between SARTre and MIRART-Trapez on the one hand and between SARTre and KOPRA/ARTS on the other are approximately the same, it should be noted, that MIRART-Trapez intensities are lower than SARTre radiances, while KOPRA and ARTS intensities are higher. Since largest deviations to MIRART are also observed at the H_2O lines, deviations are supposed to result substantially from the path integration technique. Similar behavior of ARTS and KOPRA in relation to SARTre and MIRART may, e.g., be caused by using path segment averaged quantities and solving the RTE analytically in ARTS and KOPRA vs. numerical integration techniques in SARTre and MIRART. The deviations might also be effected by limiting the maximum path lengths between grid points in ARTS and no similar feature in SARTre or MIRART.

Regarding the fine altitude resolution of the atmospheric profiles, significant deviations are observed. Nevertheless, SARTre intensities are right in between the results from MIRART-Trapez and from the other models. Considering that KOPRA and ARTS are based on identical cross sections and use similar approaches to the source integration, SARTre is found to be in fairly good agreement with the other models to continue with the intercomparison of cloud cases. Besides, contribution from emitting and scattering clouds are expected to be significantly higher than the deviations observed here.

4.4 Case II – Thermal Emission of Clouds

4.4.1 Motivation

The intercomparison of spectra resulting from thermal emission in the presence of clouds is intended to check the implementation of particles in the model. This involves the verification of the layer based treatment of particles, while properties of molecules are defined and managed on the basis of atmospheric levels (see section 3.1.3). With source terms being parameterized in terms of optical depth along the line of sight, the correct handling of particulate and molecular matter, e.g. concerning their particular effect on variation of optical properties in a single layer, may be essential to the simulated spectra.

Although a verification of the implementation of aerosols and hygrosols could have been done in a scattering case as well, it was preferred to separate and simplify the problems as far as possible. As an advantage over scattering problems, thermal emission cases are independent of the incident radiation field, i.e. they are independent of the correct solution of the radiative transfer problem in the coupled Earth-atmosphere-system. Hence, the implementation of particles in the model can be examined separately from sphericity issues.

When clouds are considered in RT calculations, extinction is due to molecular absorption as well as to absorption and scattering by particles, thus

$$\beta_\mathrm{e} = \beta_\mathrm{a}^\mathrm{mol} + \beta_\mathrm{a}^\mathrm{par} + \beta_\mathrm{s}^\mathrm{par} \qquad \text{and} \tag{4.4}$$

$$\omega_0 = \frac{\beta_\mathrm{s}^\mathrm{par}}{\beta_\mathrm{e}}. \tag{4.5}$$

Similar to the clear-sky case, here source term J only includes J_B. Consequently, the RTE is given by

$$I = I_\mathrm{dir}\,\mathcal{T}_\mathrm{dir} + \int_0^\tau (1-\omega_0)\,B(T)\,\mathrm{e}^{-\tau'}\,\mathrm{d}\tau', \tag{4.6}$$

a modified version of the Schwarzschild equation. For the thermal emission intercomparison, the setup as described in section 4.2 is used, including the two cloud types "cloud A" and "cloud S" (dominantly absorbing resp. scattering) with five scenarios of differing optical depth and five limb observation geometries. However, only SARTre and KOPRA are compared for reasons explained in section 4.1. Results for "cloud S" are shown in Fig. 4.6.

4.4.2 Results

For simulations with "basic" layer setup, i.e. only one cloud layer assumed between 9.5 – 10 km and 12 – 12.5 km, deviations between KOPRA and SARTre are found to be below ±1 % in average. Except in the center of the strong lines, almost constant differences between the models occur, when the cloud is opaque in limb (scenarios 3 to 5). Thin clouds (scenarios 1 and 2), on the other hand, show distinctive spectral signatures. Maximum deviations appear at the flanks of the strong CO_2 lines for scenario 3 of "cloud S". They reach up to −7 % for tangent altitude of 11 km and decrease with decreasing tangent height. In principle, differences in case of strong absorbing clouds are smaller than for scattering ones.

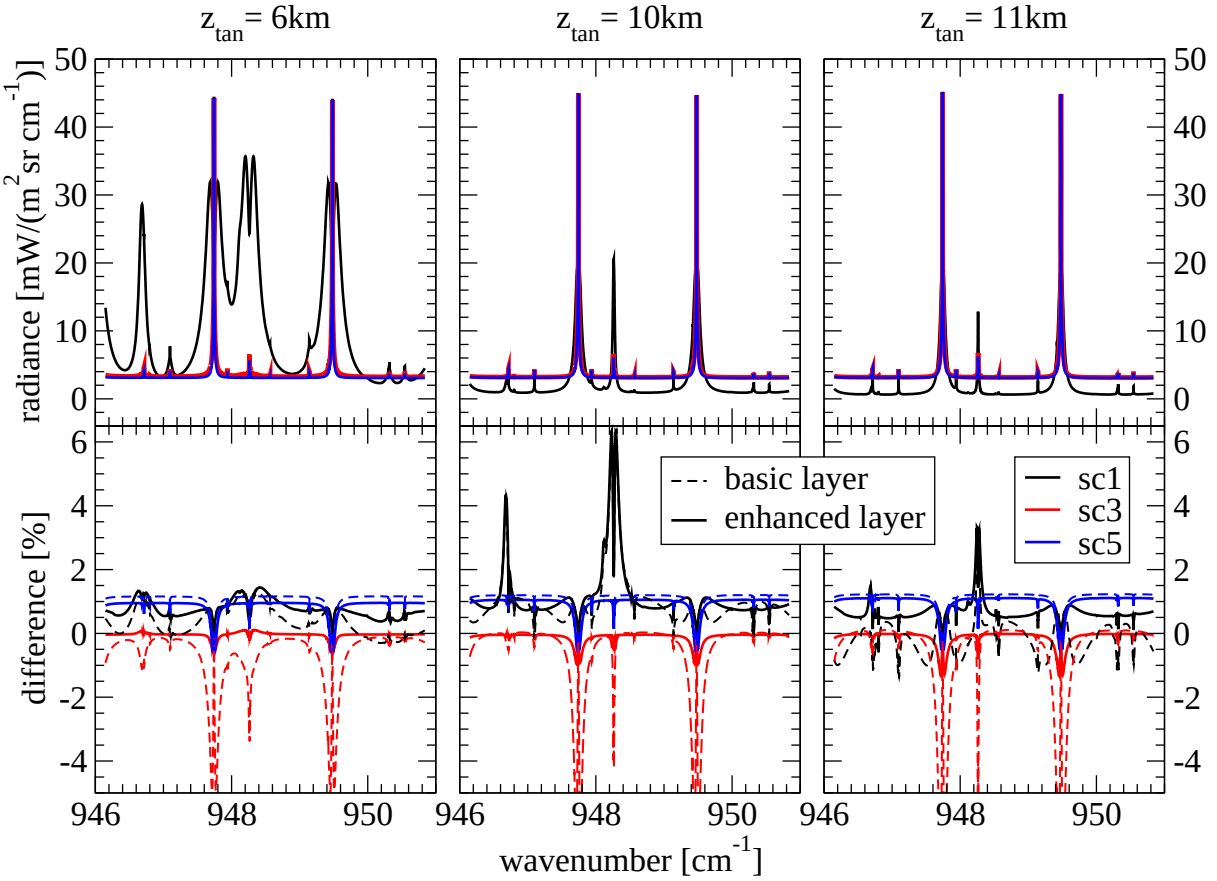

Figure 4.6: *Results of the intercomparison of RT calculations for thermal emission by clouds with "basic" (– –) and "enhanced" (——) layer setup are shown for tangent altitudes of 6 km (left), 10 km (center) and 11 km (right). SARTre intensity spectra for "cloud S" and scenarios 1, 3, and 5 are presented in the upper panel. KOPRA spectra are omitted for better perceptibility. The lower panel shows corresponding percentage deviations between SARTre and KOPRA. Maximum deviations in the* CO_2 *lines reach* −7 %.

When using the "enhanced" setup of 5 sublayers with individually fitted particle density functions, deviations become significantly smaller. Maximum differences at the CO_2 lines are reduced to below $-2\,\%$. Furthermore, spectral signatures of the deviations among with thin clouds become significantly smaller, while average deviations, e.g. for opaque clouds, retain their magnitudes.

The improvement may result from a better fit of the particle number density functions used in SARTre and KOPRA. Considering the assumption of source functions varying linearly with optical depth along the LOS (see subsection 3.1.1), the smaller deviations may further be explained by a better agreement with the linearity assumption. When a number of sublayers is used instead of a single thick layer, integration lengths of the individual path segments become smaller and the sampling rate of the source function integral is increased.

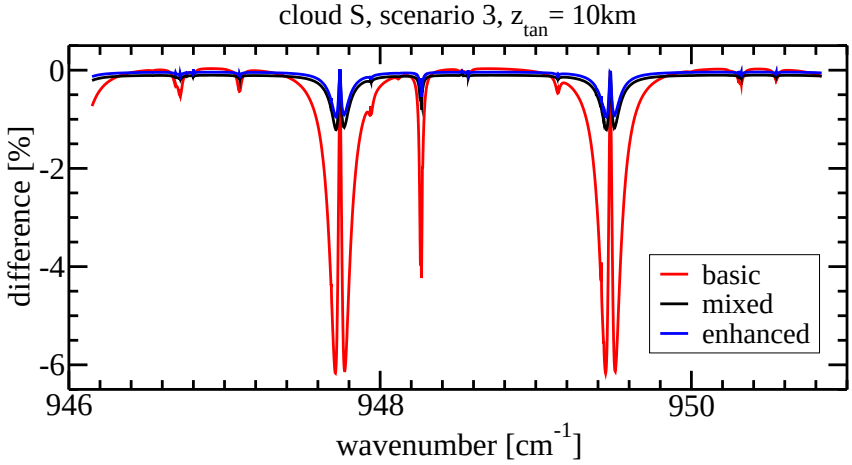

Figure 4.7: *Effects of variations in the setup of cloud layers in SARTre. Deviations of SARTre spectra and KOPRA calculations with single cloud layers of linearly increasing and decreasing particle number density are shown.*

To clarify this issue, the "mixed" setup has been applied with five sublayers, but the same density function as used for the "basic" layer setup applied to al sublayers. As can be seen from Fig. 4.7, the reduction of the deviations mainly results from including more sublayers and LOS grid points, but not from usage of more exactly fitted density functions. That implies, that the linearity assumption for the source terms is not fulfilled in case of the "basic" setup.

In particular, it has been found, that the single scattering albedo ω_0 does not satisfy the assumption with sufficient accuracy. Molecular absorption, that is almost negligible in case of optically thick clouds except for the centers of the strong lines, becomes obviously more important, when the cloud is optically thin. For thin cloud cases, molecular absorption affects the single scattering albedo noticeably. In general, molecular absorption coefficients do not vary with altitude in the same way as particle absorption and scattering coefficients. Hence, the single scattering albedo diverges strongly from linear behavior when molecular absorption is significant.

Differences observed at the flanks of the water vapor lines at tangent altitude of 10 km in case of thin clouds have not been reduced by using the "enhanced" layer setup. Reviewing Fig. 4.5 makes clear that they have already been observed in the clear-sky spectrum of the same limb geometry. As discussed in subsection 4.3 these deviation seem to be closely related to the steep increase of the water vapor content within this region of the atmosphere and can likely be ascribed to different approaches of path integration.

However, with average deviations of $\approx 1\,\%$ over the whole range of cloud types, scenarios, and observation geometries in the intercomparison, accuracy is found to be satisfactory when linearity of the source function is ensured within the single path segments. Currently, the SARTre user has to take care about this requirement by introducing a sufficient number of layers when cloud microphysical or optical properties vary fastly. For future it is suggested to implement a procedure, that supervises the linearity criterium automatically.

4.5 Scattering in SARTre – Internal Tests

4.5.1 Motivation

Before verifying the scattering part of the model by intercomparison, some internal checks are performed to SARTre. Consisting of two collaborating model parts – a spherical radiative transfer model responsible for source integration along the LOS and the plane-parallel model DISORT used to provide the diffuse radiation field needed for the calculation of multiple scattering source term J_{MS} –, SARTre has to be verified to integrate both parts in a consistent manner. Primarily this regards to the parameterization of the thermal emission source in DISORT and SARTre. Although thermal emission is implemented, DISORT is predominantly used for solar radiative transfer modeling in atmospheric science. Few references can be found that demonstrate the validity of the parameterization scheme of the Planck source term.

On the other hand, the problem of energy conservation during successive scattering events becomes apparent when modeling scattered radiation. Test cases have been defined to verify these issues. The test setups are described and results are discussed in the following subsections.

4.5.2 Consistency of Thermal Emission Sources in SARTre and DISORT

The test concerning consistency of the thermal emission source terms in SARTre and DISORT is carried out by comparing the thermal emission radiance fields calculated by both models at corresponding zenith angles. Since thermal emission is an isotropic process, no azimuthal dependency occurs and has to be considered in a 1D atmosphere. To minimize deviations resulting from different geometries, the radius of the Earth in SARTre is enlarged by a factor of 10^3, such that a quasi plane-parallel Earth-atmosphere-system is assumed. The angular grid used to compare the intensity fields is defined by discrete ordinate angles corresponding to Double Gaussian quadrature. Comparing the fields for 16 streams is considered to be sufficient, since the thermal emission radiance field is expected to show smooth angular variations in the upper and in the lower hemisphere, respectively. Furthermore, within case III of this intercomparison the solution of the scattering integral in SARTre is derived from 16-stream DISORT calculations as well, i.e intensities in DISORT are only evaluated on the same angular grid as compared here.

The setup described in section 4.2 is adapted to the current task by replacing the “cloud S” by a “blackbody” cloud with the same extinction coefficients as “cloud S”:

$$\beta_{\mathrm{e}}^{\mathrm{blackbody}} \;=\; \beta_{\mathrm{a}}^{\mathrm{blackbody}} \;=\; \beta_{\mathrm{a}}^{\mathrm{cloudS}} + \beta_{\mathrm{s}}^{\mathrm{cloudS}}. \tag{4.7}$$

Molecular absorption has not been changed. Calculations under clear-sky conditions and with cloud scenarios 1 to 5 are done at five monochromatic spectral grid points as described in subsection 4.2.1. Results for $947.6\,\mathrm{cm}^{-1}$, located in the wing of a CO_2 line, and for the continuum point at $950.2\,\mathrm{cm}^{-1}$ are shown in Fig. 4.8. The $947.6\,\mathrm{cm}^{-1}$ spectral point will also be used in section 4.6 for the radiance field intercomparison to ARTS-DOIT.

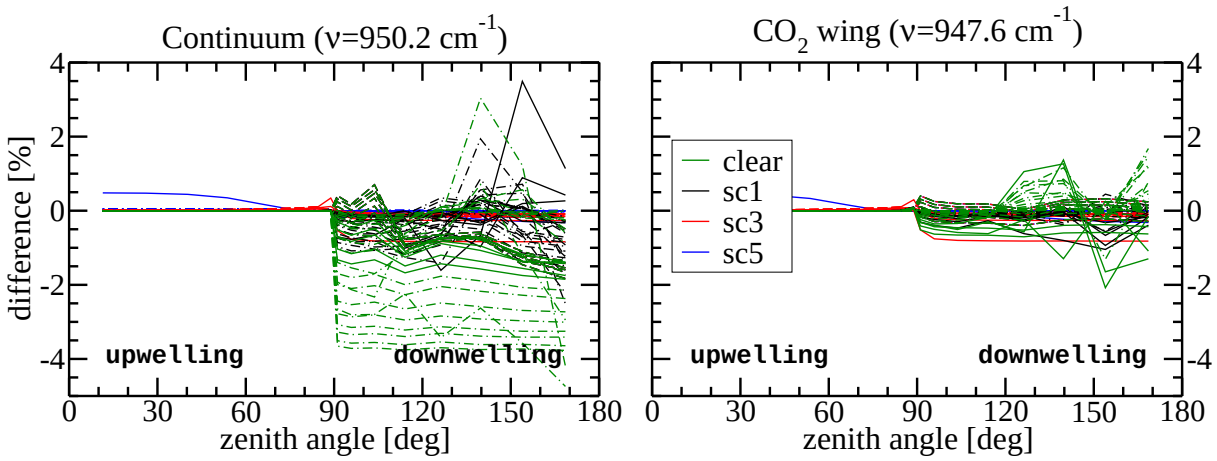

Figure 4.8: *Percentage deviations (according to Eq. (4.3)) of thermal emission radiances calculated by DISORT and SARTre in the continuum region (left) and the wing of a* CO_2 *line (right). Results are shown for clear-sky conditions and cloud scenarios 1, 3 and 5 for altitude levels (with a spacing of 0.5 km) between 8 km and 13 km below (– · –), in (——), and above (– –) the cloud.*

Upwelling radiances (zenith angle $0° \leq \theta \leq 90°$) of SARTre and DISORT, which are dominated by a strong contribution from surface emission, fit very well at all spectral grid points, scenarios, and zenith angles. The majority of differences are found to be $< 0.1\,\%$ and maximum deviations are $< 0.5\,\%$. While absolute deviations of downwelling radiation show the same magnitude as upwelling ones, relative differences are larger since contribution from the cold sky is much smaller.

Furthermore, a significant spectral dependency is observed. Largest differences occur, when the atmosphere is optically very thin. In the clear-sky case, differences are found to be between $-4\,\%$ and $+0.5\,\%$ in the continuum region and of $\pm 2\,\%$ in the wings of the lines, while deviations are below $+1\,\%$ in the H_2O line and even below $+0.05\,\%$ in the CO_2 line center. Thin cloud scenarios 1 and 2 show similar difference patterns with slightly lower deviations of $-2\,\%$ and $+1\,\%$ in the continuum and wing regions. With increasing cloud optical thickness, the spectral broadband properties of the cloud dominate and spectral dependency of the results decreases. For scenarios 3 to 5 differences are between $-0.2\,\%$ and $+0.1\,\%$ at all five spectral points. Few exceptions occur in the uppermost layers of the cloud with maximum deviations of $-1\,\%$.

In conclusion, SARTre and DISORT are found to be consistent concerning parameterization of the thermal emission source term. Both models agree the better, the thicker the medium is optically and the higher the emission source terms are. Deviations related to emission source parameterization are expected to be very low, especially since the scattering field will be dominated by the strong upwelling radiation from the surface and lower troposphere, where the results of the models fit very well.

4.5.3 Energy Conservation

When scattering is considered in radiative transfer modeling, conservation of energy is of fundamental importance. Loss or gain of energy throughout successive scattering processes has to be avoided. That means, the scattering integral Eq. (3.31) has to be evaluated with sufficient

accuracy. Furthermore, the norm of the scattering phase function needs to be conserved, in particular when expanding the phase function into Legendre terms.

Within SARTre and DISORT, integrals over polar angles are realized by using the Double Gauss quadrature method. Double Gauss quadrature combines the advantages of Gaussian quadrature[2] with a dense angular grid around the horizontal direction, where the intensities change quite abrupt. This quadrature method is supposed to yield very accurate results.

In DISORT, the phase function is used in terms of Legendre expansion coefficients χ_m (see subsection 3.4.3). For energy conservation, it is crucial to retain the norm of the phase function when transforming it into expansion coefficients. Basically, a norm of 4π is conserved, when $\chi_0 \equiv 1$. That is ensured by scaling calculated expansion coefficients by $\chi_m = \chi_m/\chi_0$ within the SARTre expansion routine, and additionally by setting χ_0 automatically to 1 in DISORT.

However, to check the correct operation of the energy conservation within the SARTre model and its DISORT module, a test case has been set up with a conservative cloud in an atmosphere without molecular absorption. Scattering coefficients and phase function of the conservative cloud are adapted from "cloud S", hence

$$\beta_{\mathrm{e}}^{\mathrm{conservative}} = \beta_{\mathrm{s}}^{\mathrm{cloudS}} \quad \text{and} \tag{4.8}$$

$$\beta_{\mathrm{a}}^{\mathrm{mol}} \equiv 0. \tag{4.9}$$

Energy conservation has been tested for the optically thickest cloud, i.e. scenario 5 cloud. Multiple scattering dominates within thick conservative clouds, where photons undergo a larger number of scattering processes.

In case of energy conservation, the net flux density

$$E_{\mathrm{net}} = \int_0^{2\pi} \mathrm{d}\phi \int_{-1}^{1} I(\theta,\phi)\, \cos\theta\, \mathrm{d}\cos\theta \tag{4.10}$$

at the bottom of the atmosphere (BOA) has to be equal to the net flux density at the top of atmosphere (TOA):

$$E_{\mathrm{net}}^{\mathrm{BOA}} = E_{\mathrm{net}}^{\mathrm{TOA}}. \tag{4.11}$$

Eq. (4.11) has been evaluated from DISORT intensity fields on 16 streams. Differences of net flux density at BOA and TOA have been found $< 0.003\,\%$, i.e. within the computational accuracy of single precision code.

For the derivation of the multiple scattering source terms J_{MS}, the scattering integral is calculated from DISORT fields by Eq. (3.36). The implementation of this equation in SARTre has been tested by calculating the scattered intensity I_{s}, represented by 16 streams, and comparing average intensities $\bar{I}_{\mathrm{i}}$ and $\bar{I}_{\mathrm{s}}$ of the incident and scattered field, respectively. From

$$\bar{I}_{\mathrm{i}} = \frac{1}{4\pi} \int_{4\pi} I_{\mathrm{i}}(\boldsymbol{\Omega})\, \mathrm{d}\boldsymbol{\Omega} \tag{4.12}$$

$$\text{and} \qquad I_{\mathrm{s}}(\boldsymbol{\Omega}) = \int_{4\pi} P(\boldsymbol{\Omega},\boldsymbol{\Omega'})\, I_{\mathrm{i}}(\boldsymbol{\Omega'})\, \mathrm{d}\boldsymbol{\Omega'}$$

$$\text{follows} \qquad \bar{I}_{\mathrm{s}} = \frac{1}{4\pi} \int_{4\pi} \int_{4\pi} P(\boldsymbol{\Omega},\boldsymbol{\Omega'})\, I_{\mathrm{i}}(\boldsymbol{\Omega'})\, \mathrm{d}\boldsymbol{\Omega'}\, \mathrm{d}\boldsymbol{\Omega}. \tag{4.13}$$

[2] Gauss showed, that in the absence of any information about the integrand, the Legendre polynomial yields optimum accuracy.

When the energy conservation principle is satisfied by the model, then $\bar{I}_\mathrm{s} = \bar{I}_\mathrm{i}$. This requirement has been met by SARTre within computational accuracy, deviations have only been found in the seventh relevant digit. In conclusion, the principle of energy conservation is realized in the SARTre model with satisfactory precision.

4.6 Case III – Scattering Intercomparison

4.6.1 Motivation

The ability to model scattering in a spherical atmosphere is one of the crucial features of SARTre. Upon evaluation of clear-sky and cloud emission cases, the following section deals with the verification of SARTre in case of scattering. For this purpose, SARTre modeling results, considering source terms J_B and J_MS in a cloudy atmosphere, are compared to radiative transfer calculations of ARTS-DOIT.

While examining limb spectra will primarily allow conclusions about the behavior of the models with respect to spectral variations, an evaluation of the pseudo-spherical approach used in SARTre can better be obtained by a comparison of radiance fields. By investigating intensity fields in and around the scattering medium, a more general conclusion may be drawn concerning the applicability of the local planarity assumption for diverse observational geometries.

Prior to the evaluation of SARTre and ARTS-DOIT radiance fields, calculated in a spherical atmosphere, intensity fields from a quasi plane-parallel atmosphere are compared. By that, it is intended to derive information about the basic agreement of the scattering implementation in the models, independently of effects resulting from different approaches in considering sphericity of the Earth and atmosphere. Setting results from a quasi plane-parallel atmosphere in contrast to those from a spherical one, deviations can clearly be attributed to sphericity issues. However, it should be considered, that sphericity issues not only include the basic concept of how sphericity is taken into account but also its implementation and the use of an appropriate setup for individual simulations.

4.6.2 Addendum to Intercomparison Setup

The atmospheric setup, described in section 4.2, has been used for the scattering intercomparison. Unless otherwise noted SARTre calculations are done using the “enhanced” layer setup, which consists of all together 15 grid points inside the cloud. First intercomparison results suggested, that the standard setup with 0.5 km thick layers does not provide sufficient accuracy for scattering calculations of ARTS-DOIT, particularly when the cloud is thick. Therefore, the altitude grid used within ARTS-DOIT for scattering calculations has been refined to an ≈ 0.06 km spaced altitude grid.

Radiance fields are calculated and compared at a single spectral grid point at $947.6\,\mathrm{cm}^{-1}$, which is located in the continuum region at higher altitudes and at the flank of a CO_2 line at lower altitudes and that has as well been included in the emission term consistency test of DISORT and SARTre (see subsection 4.5.2). Since scattering dominantly affects spectral regions of low gas absorption, results for the selected wavenumber should provide a good measure for maximum deviations resulting from scattering implementation and sphericity concepts in SARTre and ARTS-DOIT.

The angular grid of the compared radiance fields has been defined by the ARTS-DOIT grid used for scattering RT calculations in the cloud box, that had been optimized in regard

to sufficiently represent the intensity field under clear-sky conditions. It contains 129 discrete polar angles, with equidistant 10° spacing for upwelling and downwelling radiances between 0° – 80° and 100° – 180°, respectively. The spacing becomes successively smaller when approaching horizontal direction, where the intensity varies fastly with zenith angle. SARTre calculations are performed for the 129 polar angles based on 16-stream DISORT solutions.

4.6.3 Radiance Fields in a Plane-Parallel Atmosphere

Fig. 4.10 and Fig. 4.9 illustrate selected results of the comparison of radiance fields derived in a quasi plane-parallel atmosphere ($R_{\text{Earth}} = 6.37{\cdot}10^6$ km). Percentage differences of the radiance fields for "cloud A" and "cloud S" for altitudes between 8.0 km and 13.0 km plotted over polar angle are presented in Fig. 4.9. For a better understanding of spatial behavior of the deviations, Fig. 4.10 shows 2D fields of percentage deviations between SARTre and ARTS-DOIT calculations for "cloud S", plotted over zenith angle and altitude.

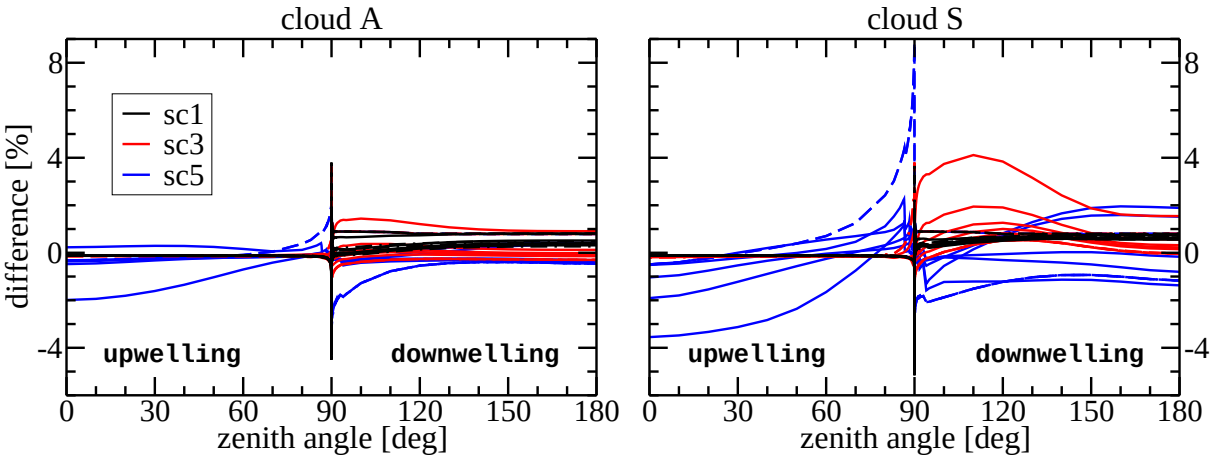

Figure 4.9: *Relative differences of ARTS-DOIT and SARTre radiance fields in a quasi plane-parallel atmosphere for "cloud A" (left) and "cloud S" (right). Results are shown for cloud scenarios 1, 3, and 5 at altitude levels between 8 km and 13 km below (– · –), in (——), and above (– –) the cloud.*

For "cloud S" deviations are generally found to be $< 1\,\%$ for upwelling radiances, except for scenario 5, where the cloud is totally opaque and the models differ between $-3.5\,\%$ in nadir in the lower part of the cloud and $+9\,\%$ in limb direction above the cloud. Deviations for scenario 5 are supposed to result from small deviations of the particle number density function used for the upper and lower layer of the cloud by ARTS-DOIT and SARTre. In case of very thick clouds this causes saturation path lengths to differ, i.e. slightly higher or lower parts of the cloud are "seen". Deviations in observed radiances result from deviations of the emission source terms around the saturation point, in particular because of the atmospheric temperature gradient.

These effects are related to (in)sufficiency of the resolution in altitude and along the line of sight, in particular to too large optical path lengths of individual path segments. When using the "basic" layer setup with only a single layer between 9.5 – 10 km and 12.0 – 12.5 km for both models, deviations reach up to 50 % resulting primarily from changes in the ARTS-DOIT solution. Maximum differences are observed in quasi horizontal direction. It is supposed, that

these are caused by slightly differing geometric conditions, since the atmosphere is quasi but not perfectly plane-parallel.

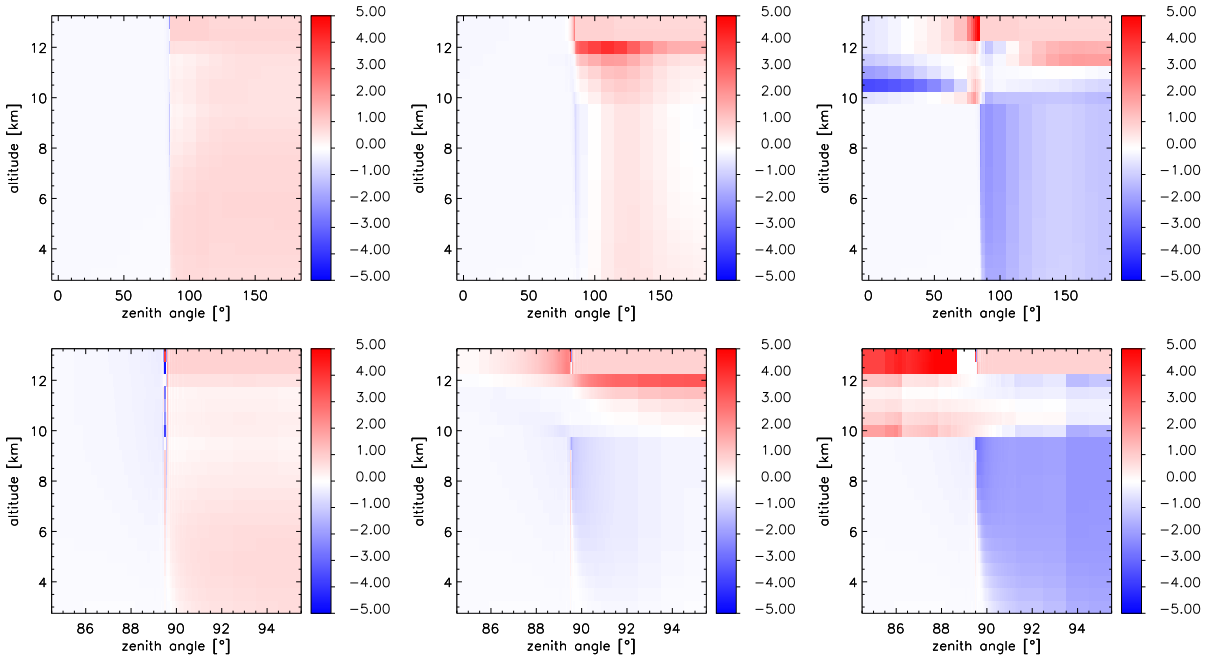

Figure 4.10: *Differences of ARTS-DOIT and SARTre radiance fields in a quasi plane-parallel atmosphere for scenarios 1 (left), 3 (middle), and 5 (right) of "cloud S". The upper panel presents difference over the whole range of zenith angles, while the lower panel shows a zoom to the horizontal direction.*

Downwelling radiances differ by about ±2 %. Slightly larger deviations are observed at zenith angles between 90° – 120° in the upper most cloud layer in scenario 2 and 3. These deviations could be caused by differences in the distribution of particle density with height, which are reduced by using the "enhanced" layer setup but not completely removed. They may further result from insufficient fulfillment of the linearity assumption, i.e. a still too coarse altitude grid in SARTre between 12 – 12.5 km. The latter explanation is supported by the fact, that for scenario 1 as well as for scenarios 4 and 5, where either molecules or particles dominate the bulk properties, this pattern is much weaker or absent.

Results for "cloud A" are similar to those of "cloud S", but deviations are smaller by a factor of ≈ 2. Downwelling radiances of scenario 5 below the cloud show deviations of the same order of magnitude as for "cloud S", which is due to slightly different saturation path lengths (see explanation for "cloud S"). In conclusion, except for optically very thick clouds, radiance fields of SARTre and ARTS-DOIT in a quasi plane-parallel atmosphere agree fairly well. The results from quasi plane-parallel solutions can be expected to represent the upper limit of achievable consilience of the spherical solutions.

4.6.4 Radiance Fields in a Spherical Atmosphere

Corresponding to Fig. 4.9 and Fig. 4.10, radiance field difference plots of over polar angles are shown for both cloud types in Fig. 4.11 and "cloud S" results are illustrated by 2D plots of percentage deviations of SARTre and ARTS-DOIT intensity fields in Fig. 4.12.

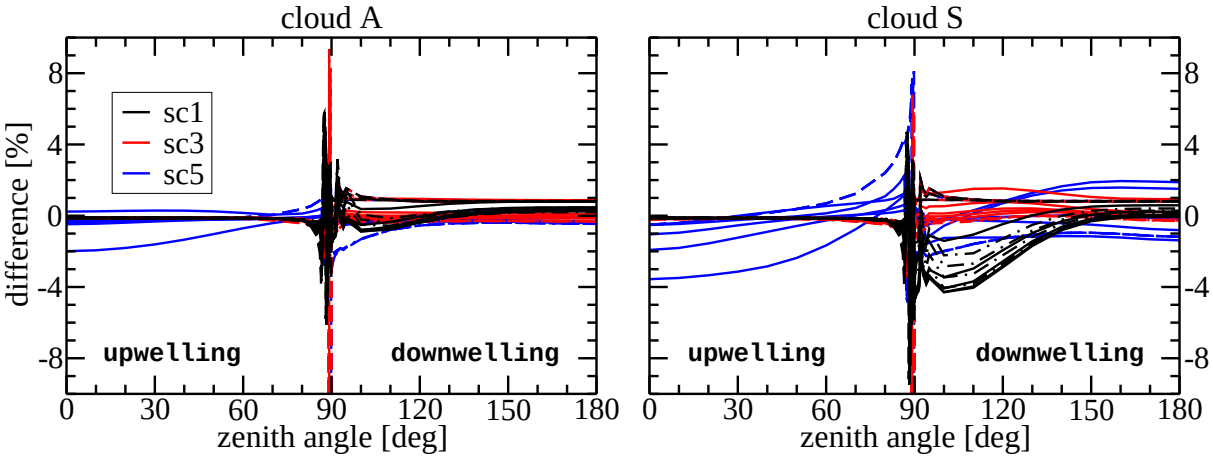

Figure 4.11: *Relative differences of ARTS-DOIT and SARTre radiance fields in a spherical atmosphere for "cloud A" (left) and "cloud S" (right). Results are shown for cloud scenarios 1, 3, and 5 at altitude levels between 8 km and 13 km below (– · –), in (——), and above (– –) the cloud.*

Upwelling intensity of zenith angles between 0° and 60° as well as downwelling radiation for zenith angles of 120° – 180° of SARTre and ARTS-DOIT are found to deviate in a similar manner to radiance fields of the quasi plane-parallel case. Sphericity of the Earth and atmosphere does not play a significant role for these observation angles.

When coming closer to horizontal direction, i.e. when atmospheric path lengths become significantly longer and local zenith angle varies noticeably along the LOS, differences to the plane-parallel case become obvious for downwelling radiation in and below "cloud S" in scenarios 1 to 3. SARTre tends to overestimate intensities in comparison to ARTS-DOIT for these thin and moderate clouds. For scenario 3, where SARTre underestimated ARTS-DOIT results slightly in the plane-parallel case, this leads to smaller deviations between the models for the spherical RT results. Except for the limb directions of $\theta = 85° \ldots 90°$, largest differences of $\approx 4\,\%$ occur around $\theta = 100°$ in scenario 1. Results for the optically thick scenarios 4 and 5 are found to be very close to those from quasi plane-parallel fields.

Illustrations of results, zoomed into horizontal and limb directions are given in the lower panel of Fig. 4.12 and by Fig. 4.13. When comparing results from the plane-parallel case (Fig. 4.10) to those from the spherical atmosphere (Fig. 4.12), it becomes obvious, that modeled contributions from thin clouds are highly dependent on the considered degree of sphericity. Modeling of spherical radiative transfer for thick and opaque clouds, on the other hand, does not lead to significant changes in modeled limb radiances. This is due to high extinction and low photon path lengths, over which local direction does not change – the local planarity assumption applies well.

A number of conspicuous deviation patterns can be observed for horizontal and limb directions in Fig. 4.13. They are clearly related to consideration of sphericity in modeling radiative transfer. That includes the approach to considering sphericity as well as the setup of the models for individual simulations.

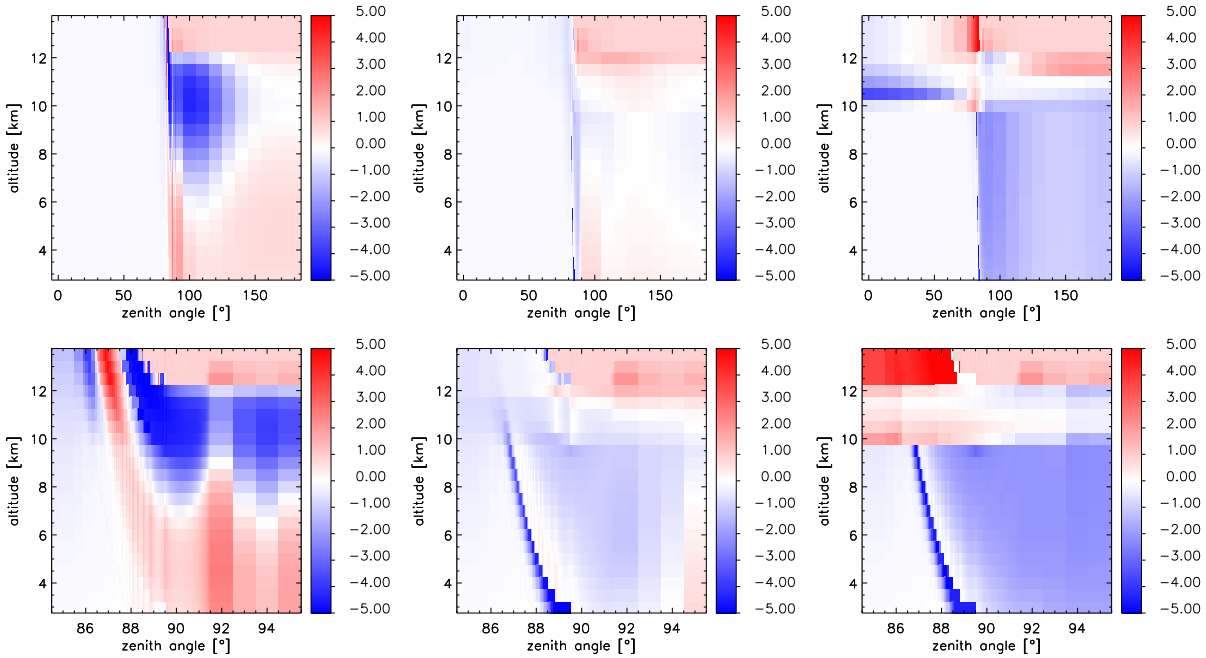

Figure 4.12: *Differences of ARTS-DOIT and SARTre radiance fields in a spherical atmosphere for scenarios 1 (left), 3 (middle), and 5 (right) of cloud B. The lower panel shows a zoom of the upper panel plots onto the region around horizontal direction.*

The difference pattern in limb direction, illustrated in Fig. 4.13 may be explained as follows:

- Pattern *1*: These oscillation like pattern result from interpolations of radiances to the optimized angular grid in ARTS-DOIT. They can be observed in all scenarios between zenith angles of 86 – 92°. Interpolations are necessary when a fixed angular grid is used in spherical atmospheres, where local zenith angles change along the path of radiation.[3]

- Pattern *2*: Large negative differences of up to −25 % (at the bottom of the cloud box at 3 km; not shown in Fig. 4.13) occur for upwelling radiation below the cloud in scenarios 3 to 5. Radiances are underestimated by ARTS-DOIT due to an inappropriate setup of the so-called cloud box. The cloud box, defined between 3 – 13 km within this intercomparison, is the part of the atmosphere, for which the scattering solution is obtained (see section 4.1.3). The scattering solution uses clear-sky radiances incident to the cloud box for boundary conditions and assumes no radiation emerging from the cloud box to reenter. However, when a 1D cloud is assumed and the atmosphere is optically thin, then the far part of the cloud is still "seen" in limb direction at the lower cloud box boundary. That means, when assuming only clear-sky incident radiation, these significant contributions from the far part of the cloud are neglected. The contributions that are missed in comparison to the SARTre solution are the larger, the thicker the cloud is. When the cloud box is extended down to the surface, this problem could be easily avoided.

[3]For more details on angular grid optimization and interpolation errors see Emde (2005)

- Pattern *3*: Significant local extrema of the deviation curve at altitudes inside and above the cloud for polar angle that correspond to limb LOS. It can be shown, that the tangent point of these viewing paths is between 9.5 – 9.6 km ($\theta = 88° - 89°$) and 12.4 – 12.5 km ($\theta = 89° - 90°$). It is furthermore observed, that deviations become larger, when the "basic" layer setup is used instead of the "enhanced", which fits well to the original linearly varying particle number density function between 9.6 – 10.0 km and 12.0 – 12.4 km. Remaining deviations are due to the worse fit for uppermost and lowermost sublayers, where original number density goes down to 0 cm^{-3}, which is impossible with exponential functions (see Fig. 4.4).

- Pattern *4*: This wave-like structure is observed in case of thin clouds (scenarios 1 and 2) at altitudes in and above the cloud for polar angles that correspond to limb observation paths. Deviations assigned to this pattern are supposed to be an effect of the pseudo-spherical approach of SARTre.

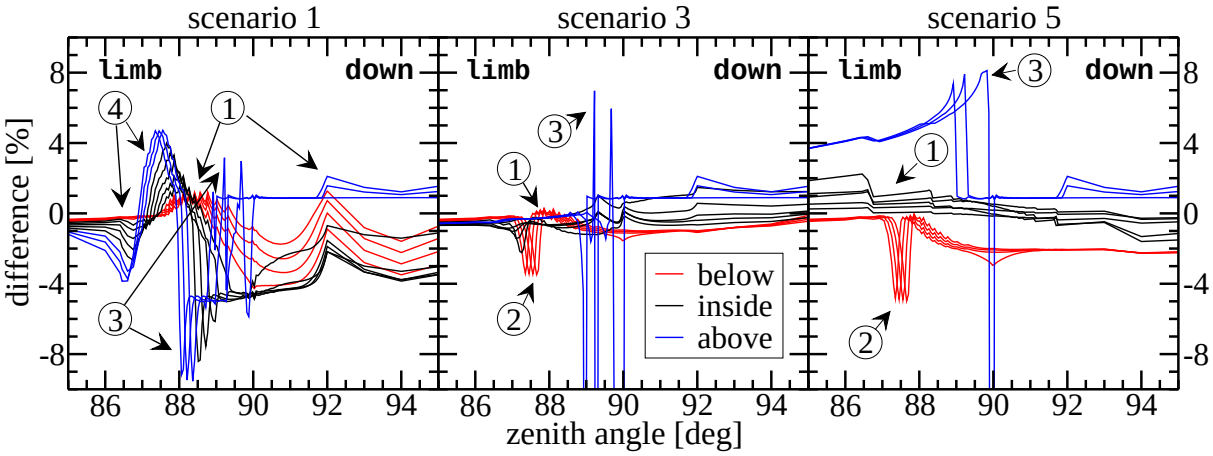

Figure 4.13: *Relative differences of ARTS-DOIT and SARTre radiance fields at near horizontal and limb directions in a spherical atmosphere for "cloud S". Results are shown at altitude levels between 8.0 km and 13.5 km for cloud scenarios 1 (right), 3 (middle), and 5 (left). Numbers denote specific difference pattern, that are explained in detail in the text.*

Pattern *4* is characterized by SARTre overestimating ARTS-DOIT results for directions corresponding to tangent altitudes between the surface and ≈ 4 km. Then, SARTre results shade off into underestimating ARTS-DOIT radiances until tangent altitudes reach the bottom of the cloud. Approaching horizontal direction, SARTre seems to switch to overestimation again, but pattern *4* is overlaid by pattern *3* within this angular interval. Maximum deviations of ±5 % are found on top of the cloud.

With no similar pattern observed in the plane-parallel case, it is highly likely, that pattern *4* is related to effects of pseudo-sphericity. Furthermore, the feature gets smaller at lower altitudes and vanishes below the cloud, where no scattering occurs. The succession of overestimation – underestimation – overestimation by the pseudo-spherical SARTre model can be explained by superimposition of – at least – two opposing effects.

On the one hand, a warm surface contributes stronger in a locally plane-parallel atmosphere. It is "seen" from nadir until horizon, while in a spherical atmosphere lines of sight close to horizon switch to limb. Beside that, the path from surface to observer or scattering point is longer in a spherical atmosphere, i.e. extinction is higher and less radiation emitted by the surface is transmitted.

On the other hand, when the path becomes longer, the amount of scattering matter along the path gets larger. Hence, with increasing path length more radiation is scattered into the path. This applies for optical path lengths of $\tau \lesssim 1$, when scattering into and out of the LOS balance each other and saturation is reached. For subvisible and thin clouds, even longest limb paths are not saturated in the examined spectral region of low molecular absorption.

Which of the described effects is dominating obviously depends on observation geometry, in particular on tangent altitude. Besides, it is likely to be related to atmospheric and surface conditions, for example on cloud location in altitude, cloud optical properties as well as molecular absorption and surface emission.

However, in case of moderate and thick clouds, optical path lengths get generally larger than $\tau = 1$ for slant paths and clouds become opaque in limb. Thus, radiance fields of scenarios 3 to 5 do not deviate noticeably for pseudo-spherical and full spherical approaches. Their difference fields completely lack the pattern *4* feature.

4.6.5 Limb Radiance Spectra

The investigation of radiance fields and differences in radiance fields between SARTre and ARTS-DOIT primarily provides knowledge about spatial and angular behavior of RT results when scattering is considered as a source of radiation. Evaluating limb spectra one derives complementary spectral information. The comparison to results of clear-sky and cloud emission simulations (see section 4.3 and 4.4) demonstrates the effect of scattering clouds on limb spectra. Selected results are presented in Fig. 4.14.

With the atmospheric and cloud setup of this intercomparison, cloud emission caused radiance enhancements between $0.5 - 4\,\mathrm{mW/(m^2\,sr\,cm^{-1})}$ for strong scattering "cloud S" (see Fig. 4.6) and $2 - 15\,\mathrm{mW/(m^2\,sr\,cm^{-1})}$ for "cloud A" in the continuum regions of the examined spectral window. When scattering is considered as source of radiation, the continuum intensity further increases to up to $22\,\mathrm{mW/(m^2\,sr\,cm^{-1})}$ for "cloud A" and $35\,\mathrm{mW/(m^2\,sr\,cm^{-1})}$ for "cloud S". From spectra shown in Fig. 4.14, it is found, that the enhancement by scattering is largest for clouds of moderate optical thickness (scenario 3), that are transparent in nadir direction but opaque in limb. Furthermore, absorption features around the H_2O lines are observed, which are characteristic to infrared limb spectra that are "contaminated" by cloud scattered radiation (for an explanation see 2.4.4).

Comparing spectra calculated by SARTre and ARTS-DOIT, results are found to agree very well for moderate clouds with deviations $< \pm 0.5\,\%$. Deviations for thick clouds are constantly $\approx 5\,\%$ in the continuum region of the spectral window. These deviations have been observed as well for plane-parallel RT simulations (see subsection 4.6.3), and are likely due to the slight differences in the cloud setup, in particular the number density parameterization.

For thin and subvisible clouds, SARTre and ARTS-DOIT results differ by up to $\pm 15\,\%$ with strong spectral and altitude variations. At tangent altitudes of 10 km and 11 km, continuum deviations dominate, while results fit well in the spectral absorption lines of both, H_2O and

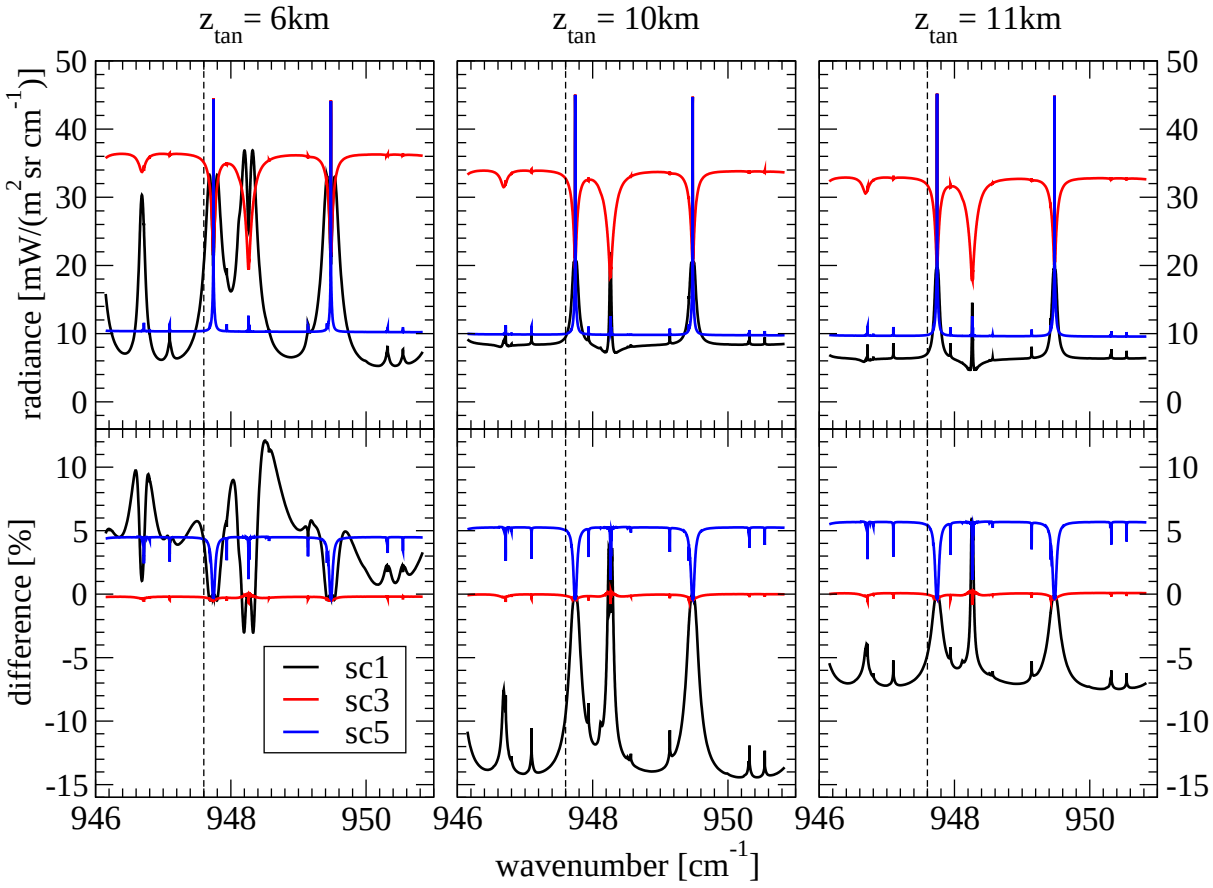

Figure 4.14: *Results of the intercomparison of scattering limb spectra for tangent altitudes of 6 km (left), 10 km (center) and 11 km (right). SARTre intensity spectra are presented in the upper panel for "cloud S" and scenarios 1, 3 and 5. ARTS-DOIT spectra are omitted for better perceptibility. The lower panel shows corresponding percentage deviations between SARTre and ARTS-DOIT. Vertical black lines indicate the wavenumber of examined radiance fields.*

CO_2. From radiance field investigation (see discussion of pattern *3* in the previous subsection and Fig. 4.15), it is known, that the large deviations for $z_{\tan}$= 10 km result from differences in the cloud setup. For $z_{\tan}$= 11 km the overestimation of the intensity by SARTre of $\approx 7\,\%$ is due to the pseudo-spherical approach of SARTre. Deviations for $z_{\tan}$= 6 km can be explained by differences in clear-sky modeling (compare to Fig. 4.5 in section 4.3), overlaid by sphericity effects (compare to Fig. 4.15).

In contrast to clear-sky and cloud emission results for "cloud S", largest deviations occur in the continuum region instead of in the spectral absorption lines. This is because contributions from cloud scattering as well as emission dominate over trace gas contributions. In conclusion, deviations due to the pseudo-spherical approach of SARTre may account for up to $\pm 10\,\%$ in continuum regions when scattering is very strong. While for tangent altitudes in the upper troposphere continuum intensities are overestimated, SARTre spectra for middle troposphere limb measurements underestimate "true" spherical spectra. Pseudo-spherical and spherical RT results agree significantly better for absorbing clouds than for strong scattering ones.

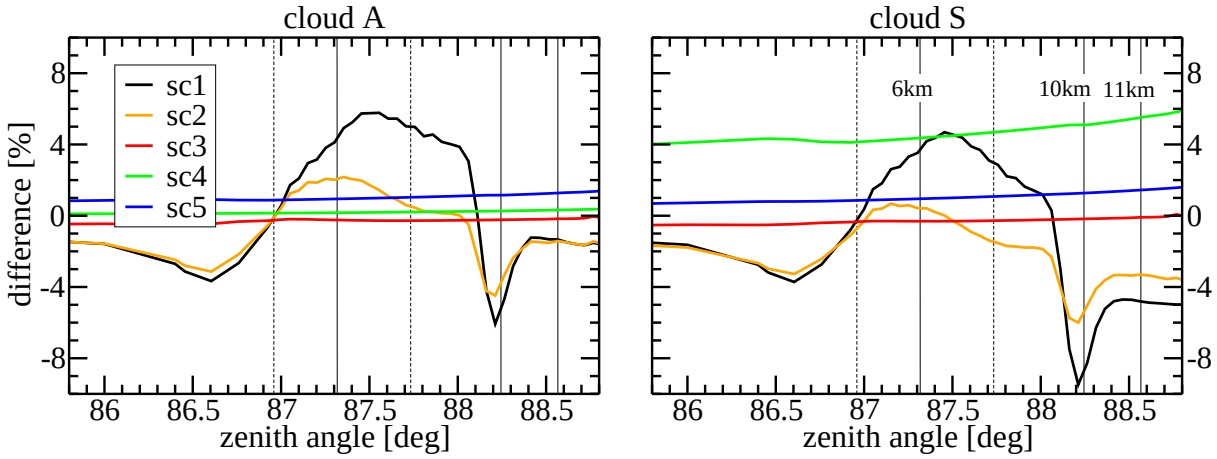

Figure 4.15: *Deviations of SARTre and ARTS-DOIT radiance fields at the altitude level of 13 km for scenarios 1 to 5 for "cloud A" (left) and "cloud S" (right) for limb observation directions above the cloud. Vertical black lines indicate the directions for tangent altitudes of 4 km, 6 km, 8 km, 10 km, and 11 km.*

4.7 Summary

By intercomparing SARTre to three packages for radiative transfer calculations in the infrared and microwave spectral range, MIRART, KOPRA, and ARTS, it has been possible to verify terrestrial RT modeling by SARTre. It has been found, that SARTre clear-sky simulations agree within the accuracy of the other models, that have been compared to each other in previous studies (von Clarmann et al., 2002; Melsheimer et al., 2005).

When considering clouds, or particulate matter in general, the importance of representing optical properties of the mixed medium has been demonstrated. Usually gaseous and particulate matter behave very different concerning spatial distribution as well spectral properties. With regard to the assumption of source terms varying linearly with optical depth along the line of sight, optical properties of the joint medium have to vary approximately linearly within individual path segments. This requirement is commonly met, when either particles or trace gases dominate the optical properties. In case of both media having significant impact on joint properties, linearity has to be ensured by choosing path segments appropriately short. Currently, this can only be controlled via the atmospheric profile grid and cloud layer definition provided as input data to SARTre. No checks and automatic adjustment are implemented yet.

The pseudo-spherical approach, that is used by SARTre when scattering is considered, has been demonstrated to yield good agreement to full spherical radiative transfer, when the cloud optical thickness is sufficiently high, i.e. when the cloud is opaque in limb and slant direction (for zenith angles of $\theta \geq 70°$). Sphericity of the atmosphere gets an evident impact with decreasing cloud optical thickness. However, it has been observed that slight changes in the intercomparison setup can cause significant deviations as well as changes in the individual model setup of each calculation.

In conclusion, SARTre is found to be an appropriate tool for modeling infrared and microwave radiative transfer in spherical atmospheres with scattering taken into account.